Annual Methodological Archive Research Review
http://amresearchreview.com/index.php/Journal/about
Volume 3, Issue 12 (2025)

Online ISSN 3007-3197
Print ISSN 3007-3189

http://amresearchreview.com/index.php/Journal/about

# Numerical Simulations to Investigate The Lift And Drag vs Angle of Attack for NACA 4412 Airfoil

**Muhammad Zahid**
Department of Mathematics and statistics, University of Southern Punjab, Multan, Pakistan Email: muhammadzahid82@gmail.com

**Sajad Hussain**
Department of Mathematics and statistics, University of Southern Punjab, Multan, Pakistan Email: sajjadhussainranahot@gmail.com

**Muhammad Rashid Iqbal** (Corresponding author)
Department of Mathematics and statistics, University of Southern Punjab, Multan, Pakistan Email: rashidiqbalkhan554@gmail.com

## ABSTRACT

This research examines the aerodynamic behavior of a NACA 4412 airfoil under subsonic flow conditions. The behavior is examined in term of lift and drag and lift-drag ratio which are produced because of air attacking the airfoil. For a C-type geometry, lift is calculated against different values of angle of attack and different values of inlet velocity. The mathematical model comprises the two-dimensional continuity and Navier-Stokes equations along with the two additional equations of Standard k-ε turbulence model to capture the turbulence. The equations in the model are a set of nonlinear partial differential equations to be solved simultaneously. For this, we use finite volume method which a part of Fluent solver. All the tasks are performed on ANSYS Workbench.

**Keywords:** NACA 4412 Airfoil; Angle Of Attack; Lift Coefficient; Drag Coefficient; CFD

## Introduction

The study of aerodynamics plays a fundamental role in designing an efficient and stable flight systems. One of the critical parameters for determining the performance of an airfoil is the angle of attack, which is the angle between the chord line of the airfoil and the direction of the airflow. The NACA 4412 airfoil, a member of the NACA 4-digit series, is widely used due to its moderate aerodynamic efficiency and good lift-to-drag ratio. It is a versatile design with applications in both low and moderate-speed regimes of flight, where it provides a balance between stability and efficiency [1-2]. In aerodynamics, the lift generated by an airfoil is the force that acts perpendicular to the

Online ISSN 3007-3197
Print ISSN 3007-3189



flow, enabling an aircraft to remain airborne, while drag is the resistive force that acts opposite to the motion. The aerodynamic performance of an airfoil is significantly influenced by the angle of attack. As the angle increases, lift generally increases until a critical angle is reached, beyond which flow separation causes a loss in lift and an increase in drag [3-4]. The study of this relationship between lift and drag with respect to the angle of attack is crucial for understanding the efficiency and stability of an airfoil [5]. Traditionally, wind tunnel testing has been used to investigate the aerodynamic properties of airfoils. However, this method is often time-consuming and expensive. In recent years, computational fluid dynamics (CFD) has become a popular alternative for simulating fluid flow around airfoils, offering a more efficient and cost-effective solution [6]. CFD uses numerical methods to solve the governing equations of fluid dynamics, particularly the Navier-Stokes equations, which describe the behavior of the fluid flow [7-8]. This allows for a detailed analysis of the airflow around the airfoil surface and the computation of forces such as lift and drag [9-10]. The NACA 4412 airfoil has been widely studied using CFD to predict its performance at various angles of attack. Previous studies have shown that the lift and drag coefficients vary significantly with the angle of attack, and these variations are crucial for determining optimal flight conditions [11-12]. CFD simulations can capture the effects of boundary layer**,** flow separation**,** and pressure distribution over the airfoil, which are difficult to measure experimentally [13-14]. Moreover, CFD allows for the simulation of different flow conditions, including variations in Reynolds number**,** Mach number, and turbulence models to evaluate the airfoil's performance under various operating conditions [15-16]. A key benefit of CFD simulations is the ability to model airfoils in conditions that would be difficult to reproduce in a physical wind tunnel. For instance, the impact of turbulence**,** compressibility effects**,** and high angles of attack can be accurately assessed using numerical methods [17-18]. Additionally, CFD provides a more comprehensive understanding of the interaction between the airfoil surface and the surrounding airflow, offering insights into phenomena such as flow separation and the development of shock waves at higher speeds [19-20]. By investigating the lift and drag characteristics of the NACA 4412 airfoil through numerical simulations, it is possible to identify the optimal angle of attack that maximizes lift while minimizing drag. This angle is critical for achieving efficient aerodynamic performance, particularly in the design of wings for aircraft [21-22]. Furthermore, understanding how the drag coefficient changes with respect to the angle of attack can help engineers to design airfoils that offer better fuel efficiency and overall performance [23-24]. In the numerical simulations, the relationship is established between lift**,** drag, and the angle of attack for the airfoils while the primary objective is to determine the angle of attack at which the airfoil achieves its best aerodynamic performance in terms of lift-to-drag ratio, and to analyze how the aerodynamic forces vary across a range of angles of attack [25].

This current study examines how a NACA 4412 airfoil behaves at various attack angles, ranging from 1° to 40° along with the associated lift and drag forces acting on the airfoil, the distribution of static pressure and velocity profiles development. For this purpose, contours graphs are analyzed for each scenario. A plot showing how the lift coefficient (CL) and drag coefficient (CD) change as the angle of attack changes is also included

Annual Methodological Archive Research Review
http://amresearchreview.com/index.php/Journal/about
Volume 3, Issue 12 (2025)

Online ISSN 3007-3197
Print ISSN 3007-3189

http://amresearchreview.com/index.php/Journal/about

in the analysis.

**Problem Statement**

This study examines how a NACA 4412 airfoil behaves (AD)ally at various attack angles, ranging from 1° to 40° along with the associated lift and drag forces acting on the airfoil, the distribution of static pressure and velocity profiles are analyzed through the contour plots for each scenario. A plot showing how the lift coefficient (CL) and drag coefficient (CD) change as the angle of attack changes is also included in the analysis.

**Computational Geometry**

The computational domain for computations is a C-type geometry as shown in Fig. 1. The circular arcs on the left side are the velocity inlet while the vertical line on the right side is the pressure outlet. The horizontal lines attached to the outlet are symmetry lines. The computational domain is the fluid (air) zone only. The airfoil body is a solid body and hence it is not the part of the computational domain, rather it is present as a solid boundary. The length of the airfoil is 1 m. We create the computational geometry in ANSYS DesignModeler. The radius of the circular arcs is 3m, the length of the symmetry line is 3 m and the length of the outlet is 6 m.

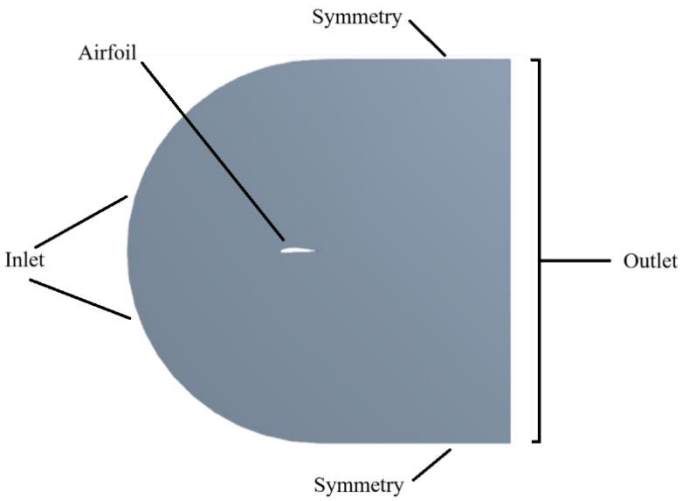



Fig. 1 Computational domain

The NACA 4412 profile sketch is given below.

Annual Methodological Archive Research Review
http://amresearchreview.com/index.php/Journal/about
Volume 3, Issue 12 (2025)

Online ISSN 3007-3197
Print ISSN 3007-3189

http://amresearchreview.com/index.php/Journal/about

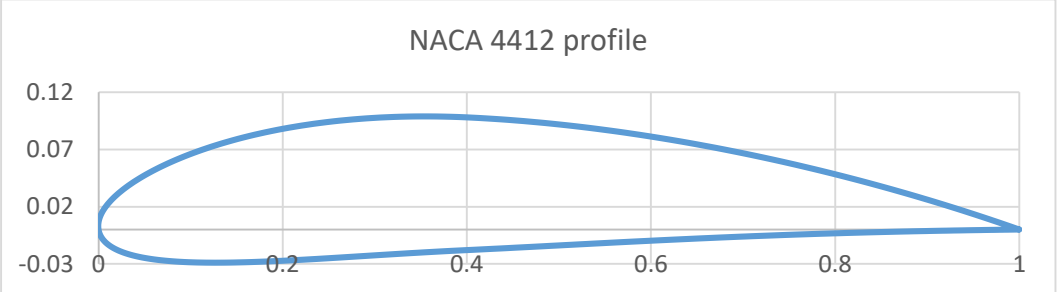



Fig. 2 NACA 4412 airfoil profile

**Mathematical Model**

The mathematical model comprises the flow and the turbulence models which are given in the following subsections.

**Flow Model**

The flow model contains the two-dimensional continuity and the Navier-Stokes equations for a steady and incompressible flow given as follows:

$$\frac{\partial u}{\partial x}+\frac{\partial v}{\partial y}=0 \tag{1}$$

The momentum equations for viscous flow in the x and y directions are as follows:

$$\rho\left(\frac{\partial u}{\partial t}+u\frac{\partial u}{\partial x}+v\frac{\partial u}{\partial y}\right)=-\frac{\partial \rho}{\partial x}+\rho\delta_x+\mu\left(\frac{\partial^2 u}{\partial x^2}+\frac{\partial^2 u}{\partial y^2}\right) \tag{2}$$

$$\rho\left(\frac{\partial v}{\partial t}+u\frac{\partial v}{\partial x}+v\frac{\partial v}{\partial y}\right)=-\frac{\partial \rho}{\partial x}+\rho\delta_y+\mu\left(\frac{\partial^2 v}{\partial x^2}+\frac{\partial^2 v}{\partial y^2}\right) \tag{3}$$

**Turbulence Model**

We use Standard k-ϵ turbulence models for capturing the turbulence in the flow. This model contains two additional transport equations which are simultaneously solved with the flow model. These equations are

$$\frac{\partial}{\partial t}(\rho k)+\frac{\partial}{\partial x_i}(\rho k\mu_t)=\frac{\partial}{\partial x_i}\left[\mu+\left(\frac{\mu_t}{\sigma_k}\right)\frac{\partial k}{\partial x_i}\right]+G_k+G_b-\rho\epsilon-Y_M+S_k \tag{4}$$

$$\frac{\partial}{\partial t}(\rho k)+\frac{\partial}{\partial x_i}(\rho\epsilon\mu_t)=\frac{\partial}{\partial x_i}\left[\mu+\left(\frac{\mu_t}{\sigma_\epsilon}\right)\frac{\partial}{\partial x_i}\right]+C_{1\epsilon}\frac{\epsilon}{k}(G_b)-C_{2\epsilon}\rho\frac{\epsilon^2}{k}+S_\epsilon \tag{5}$$

**Discretization**

We use the finite volume method to solve our flow model. This method discretizes the partial differential equations on each finite volume converting them into system of linear algebraic equations to be solved simultaneously.

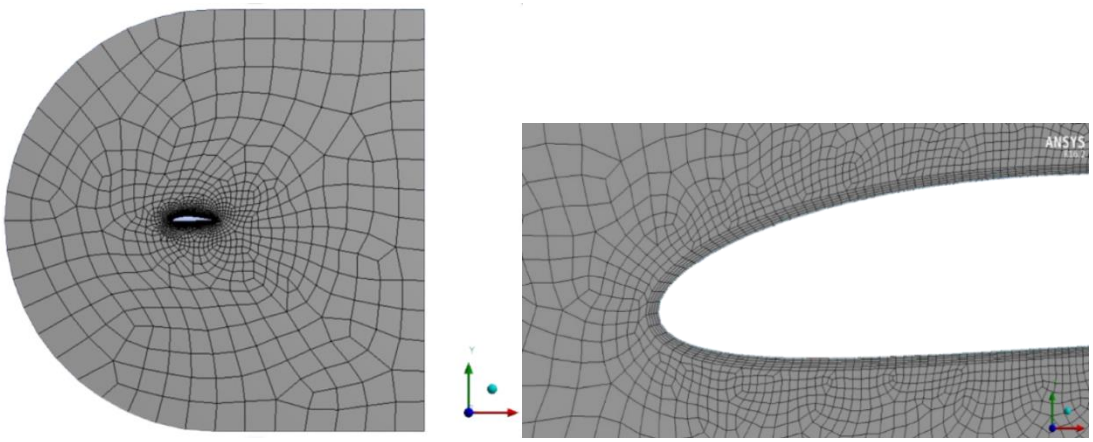
**Meshing**

Annual Methodological Archive Research Review
http://amresearchreview.com/index.php/Journal/about
Volume 3, Issue 12 (2025)

Online ISSN 3007-3197
Print ISSN 3007-3189

http://amresearchreview.com/index.php/Journal/about

In order to use the finite volume method, the computational domain must be discretized into smaller volumes. In our computational mesh, there are 8066 nodes and 7784 elements with an average skewness of 0.73215, an average aspect ratio of 2.2867 and an average orthogonal quality of 0.96533. The mesh of the computational domain is shown in Figures 3.




(a) (b)

Fig. 3. (a) Computational mesh and (b) zoomed view of mesh around the airfoil nose.

**Coefficient of Lift and Coefficient of Drag**

The lift coefficient is calculated using the relation given below

$$C_L = \frac{\text{Lift force}}{0.5\rho V^2 A} \quad (6)$$

The dynamic pressure q is equal to $0.5\rho V^2$. Hence, the above equation takes the form

$$C_L = \frac{L}{qA} \quad (7)$$

The drag coefficient $C_D$ is dimensionless measurement used in aerodynamics to quantify the resistance an item faces when travelling through a fluid. $C_D$ can be calculated by the equation,

$$C_D = \frac{\text{Drag force}}{0.5\rho V^2 A} \quad (8)$$

The above equation may be written as

$$C_D = \frac{D}{qA} \quad (9)$$

The drag force, a measure of the resistance opposing an object's motion, can be calculated using the formula: Drag Force = $C_D \times 0.5 \times \rho \times A \times V^2$. In this equation, ρ represents the density of the fluid, A is the reference area of the object, and V denotes the velocity of the object relative to the fluid. This fundamental concept is crucial in understanding the dynamics of fluid motion and its impact on objects moving through it. $C_D$ = Drag Coefficient.

**Results and Discussion**

In the current study, we investigate the impact of the $\boldsymbol{\alpha}$ and inlet velocity on the

Annual Methodological Archive Research Review
http://amresearchreview.com/index.php/Journal/about
Volume 3, Issue 12 (2025)

Online ISSN 3007-3197
Print ISSN 3007-3189

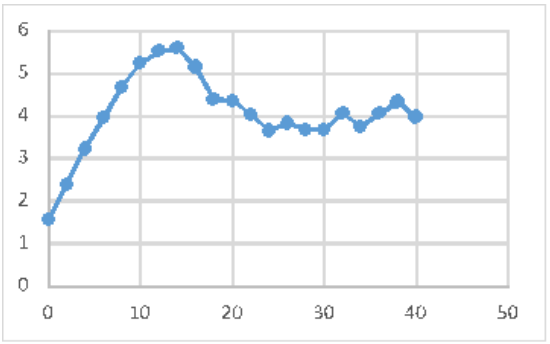
http://amresearchreview.com/index.php/Journal/about

coefficient of lift $C_L$, coefficient of drag $C_D$ and their ratio $C_L/C_D$. The $\alpha$ varies from $0^0$ to $40^0$ with a gap of $2^0$. In Fig. 4 (a), The five graphs illustrate the relationship between the lift coefficient and velocity at different speeds, showing how the lift changes as velocity increases from 2 m/s to 10 m/s. For graph (a), starts with a low lift coefficient around 2, gradually rises to a peak at approximately 10, and then slightly decreases, stabilizing around 8 to 10. This indicates that at lower velocities, the lift increases initially but levels off after a certain point. For graph (b), starts at a higher lift coefficient, around 3 to 4, and increases more sharply, reaching a peak near 17-18. After this peak, it drops slightly but remains stable around 15-16, showing a more significant response to increasing velocity compared to 2 m/s. For graph (c), the lift coefficient starts at around 10, rises rapidly, and reaches a high peak near 40. After this peak, the curve fluctuates between 30 and 40, indicating that at higher velocities, the aerodynamic behavior becomes more variable. In the graph (d), the curve starts with a lift coefficient of about 20-25, rises sharply to a peak around 65-70, and then fluctuates between 60 and 70. This graph demonstrates more dramatic fluctuations in the lift coefficient, suggesting that at these higher velocities, the system's lift becomes less predictable. The graph(e) starts with a high lift coefficient of 40-50, increases steadily to a much higher peak around 120-130, and then drops significantly, fluctuating between 100-120. This suggests that at very high velocities, the lift coefficient experiences greater instability, with significant variations after reaching the peak. A similar pattern is observed in the other graphs of Fig. 4, i.e., Fig. 4 (b), (c), (d) and (e). In Fig. 5 (a), In the five graphs, the relationship between drag coefficient **(**CD**)** and velocity is depicted at different speeds. In graph (a), at 2 m/s, the CD starts at a low value and increases gradually, reaching a maximum of around 3.5 at 40 m/s. In graph (b), at 4 m/s, the CD starts slightly higher and rises more steeply, reaching a value of about 12 at 40 m/s. Moving to graph (c) at 6 m/s, the drag coefficient starts at around **2** and increases sharply, reaching a value of 35 at 40 m/s. In graph (d), at 8 m/s, the CD starts at 4 and rises even more steeply, peaking at around 60. Finally, in graph (e), at 10 m/s, the CD begins at 5 and increases rapidly, reaching nearly 100 at 40 m/s. As the velocity increases from 2 m/s to 10 m/s, the CD increases more sharply, with the highest increase observed at 10 m/s.A similar pattern is observed in the other graphs of Fig. 5, i.e., Fig. 5 (b), (c), (d) and (e).

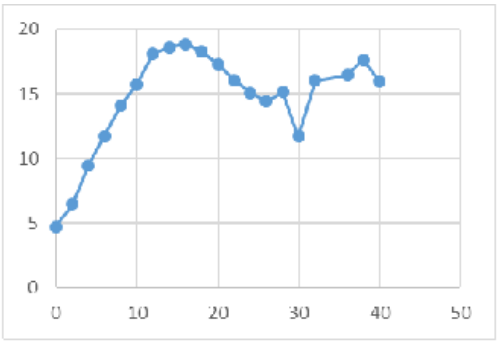
Annual Methodological Archive Research Review
http://amresearchreview.com/index.php/Journal/about
Volume 3, Issue 12 (2025)

Online ISSN 3007-3197
Print ISSN 3007-3189

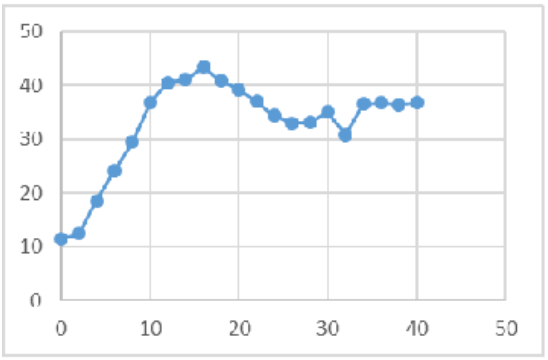
http://amresearchreview.com/index.php/Journal/about



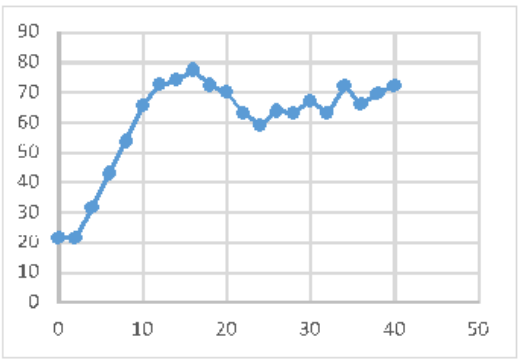

(a) Lift Coefficient with velocity 2ms-1



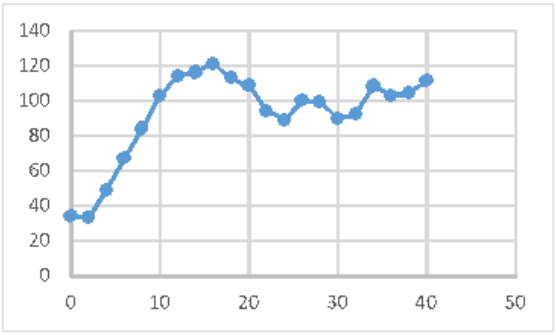

(b) Lift Coefficient with velocity 4ms-1




(c) Lift Coefficient with velocity 6ms-1




(d) Lift Coefficient with velocity 8ms-1

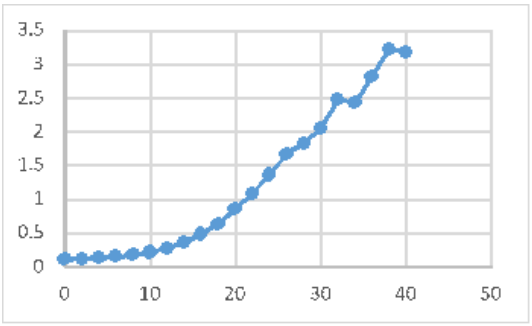



(e) Lift Coefficient with velocity 10ms-1

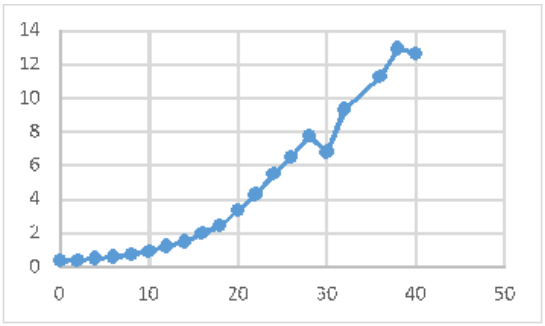
Fig. 4. Coefficient of lift $C_L$ against $\alpha$ for inlet velocity (a) u = 2 m/s, (b) u = 4 m/s, (c) u = 6 m/s, (d) u = 8 m/s and (e) u = 10 m/s

Annual Methodological Archive Research Review
http://amresearchreview.com/index.php/Journal/about
Volume 3, Issue 12 (2025)

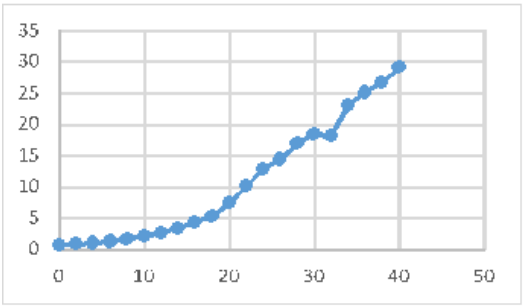
Online ISSN 3007-3197
Print ISSN 3007-3189
http://amresearchreview.com/index.php/Journal/about



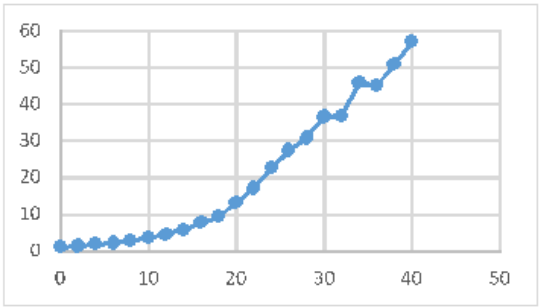

(a) (CD) by velocity 2ms-1



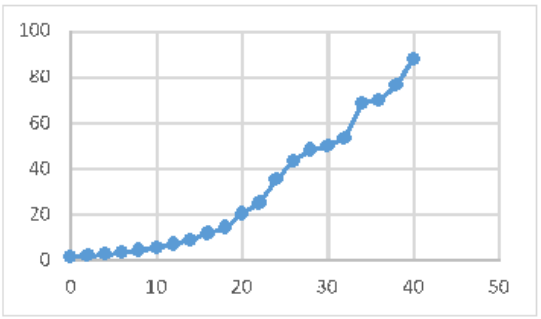

(b) (CD) by velocity 4ms-1




(c) (CD) by velocity 6ms-1




(d) (CD) by velocity 8ms-1




(e) (CD) by velocity 10ms-1

Fig. 5. Coefficient of drag $C_D$ against $\alpha$ for inlet velocity (a) u = 2 m/s, (b) u = 4 m/s, (c) u = 6 m/s, (d) u = 8 m/s and (e) u = 10 m/s

The lift-to-drag ratio (L/D or $C_L/C_D$) evaluates an airplane's aerodynamic performance, as it represents the relationship between the aerodynamic forces of lift and drag. Geodynamicists use the term "lift to drag ratio (L/D or $C_L/C_D$)" to quantify this relationship. A high L/D (or $C_L/C_D$) ratio indicates that an airplane has significant lift and minimal drag.

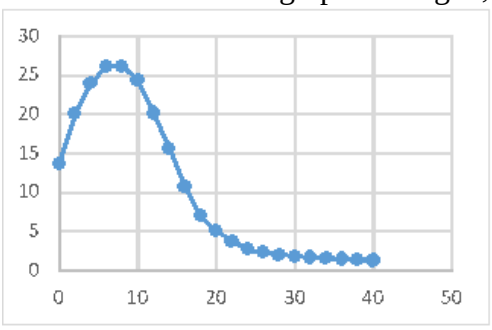
In Fig. 6(a), In all five graphs, the CL/CD ratio starts at a relatively high value at 0° (ranging from 16 to 25**)** and then decreases sharply as the angle of attack increases. In graph (a)**,** with a velocity of 2 m/s, the ratio starts around 25 and drops rapidly until it stabilizes around 1.5 to 2 by 40°**.** In graph (b) at 4 m/s, the ratio starts at 22, decreases sharply, and stabilizes around 2 at 40°**.** In graph (c) at 6 m/s, the ratio begins at 20,

Annual Methodological Archive Research Review
http://amresearchreview.com/index.php/Journal/about
Volume 3, Issue 12 (2025)

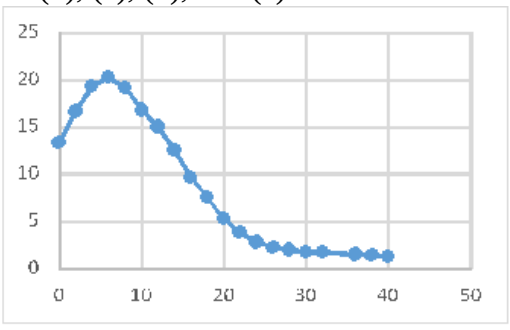
Online ISSN 3007-3197
Print ISSN 3007-3189

http://amresearchreview.com/index.php/Journal/about

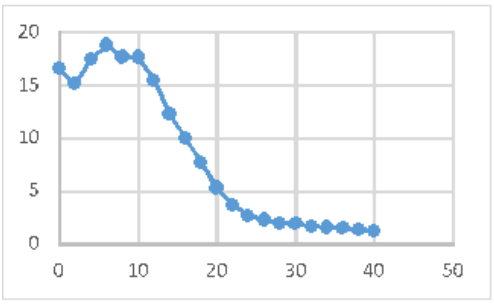
experiences a sharp decline, and then flattens to about 1 by 40°. Similarly, in graph (d) at 8 m/s, the ratio starts at 18, decreases sharply, and stabilizes around 1.5 at 40°. Lastly, in graph (e) at 10 m/s, the ratio starts at 16, drops rapidly, and stabilizes around 1 to 1.5 by 40°**.** Across all the graphs, the CL/CD ratio decreases most rapidly from 0° to 10°**,** after which it gradually stabilizes around a lower value by 40°. A similar pattern is observed in the other graphs of Fig. 6, i.e., Fig. 6 (b), (c), (d), and (e).



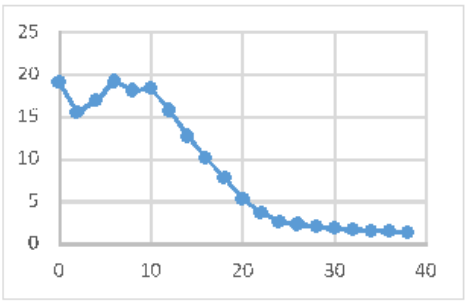

(a) Ratio CL/CD with velocity 2ms-1



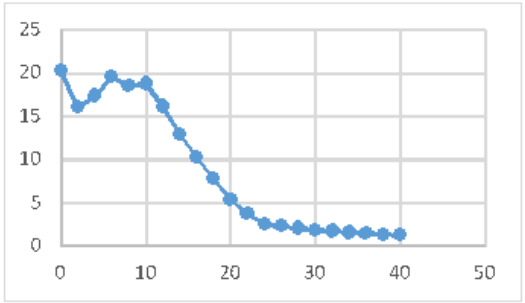

(b) Ratio CL/CD with velocity 4ms-1




(c) Ratio CL/CD with velocity 6ms-1




(d) Ratio CL/CD with velocity 8ms-1




(e) Ratio CL/CD with velocity 10ms-1

Fig. 6. $C_L/C_D$ against $\boldsymbol{\alpha}$ for inlet velocity (a) u = 2 m/s, (b) u = 4 m/s, (c) u = 6 m/s, (d) u = 8 m/s and (e) u = 10 m/s

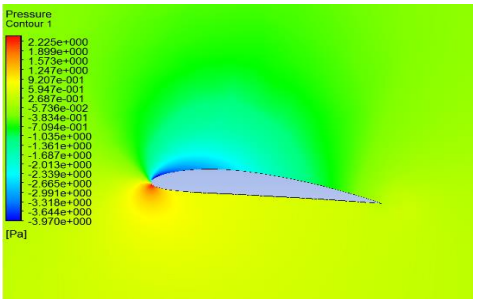
To analyze the local aerodynamic behavior against the airfoil, it is important to visualize contours for different parameters. It is important to see the impact of the air pressure on the airfoil. In Fig. 7(a), In the five graphs, each showing the contour of static pressure at an angle of attack (AOA) of 6°, we observe how the static pressure distribution changes with increasing velocity. In graph (a) with a velocity of 2 m/s, the

Annual Methodological Archive Research Review
http://amresearchreview.com/index.php/Journal/about
Volume 3, Issue 12 (2025)

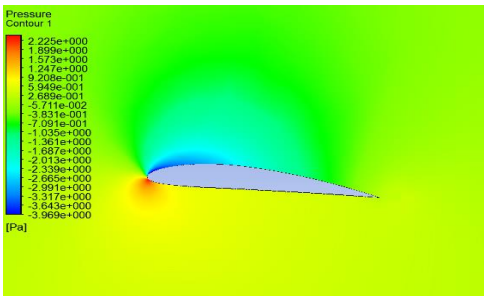
Online ISSN 3007-3197
Print ISSN 3007-3189

http://amresearchreview.com/index.php/Journal/about

static pressure is highest near the leading edge, and it gradually decreases towards the trailing edge, with a noticeable drop indicating flow separation. In graph (b) at 4 m/s, the pressure gradient becomes more pronounced, and the flow separation point is more defined. At 6 m/**s** in graph (c)**,** the static pressure continues to decrease sharply over the airfoil, with a more noticeable drop near the trailing edge and clearer flow separation. In graph (d) at 8 m/s, the pressure drop becomes even sharper, and the low-pressure region expands, indicating stronger flow separation. Finally, in graph (e) at 10 m/s, the static pressure drop is most severe, with the low-pressure region extending further, showing significant flow separation and turbulent flow over the airfoil. As velocity increases, the static pressure gradient steepens, and flow separation becomes more pronounced, indicating increasing aerodynamic effects and turbulence. This behavior may be seen in Fig. 8(a). In the five graphs showing the contour of static velocity at an angle of attack (AOA) of 6°, we observe how the velocity distribution changes with increasing speed. In graph (a)**,** with a velocity of 2 m/s, the velocity is lowest near the leading edge and increases gradually towards the trailing edge. As the velocity increases to 4 m/s in graph (b)**,** the flow velocity around the airfoil increases slightly, with the gradient becoming slightly steeper. In graph (c**)** at 6 m/s, the velocity is higher across the surface, especially near the upper surface of the airfoil, and the velocity gradient becomes more pronounced. With 8 m/s in graph (d)**,** the velocity distribution becomes even sharper, with faster flow and a more distinct velocity gradient. Finally, in graph (e) at 10 m/s, the flow velocity is highest, with a clear spread of high-velocity regions across the surface, indicating a more turbulent flow and sharper velocity gradients. Overall, as the velocity increases from 2 m/s to 10 m/s, the flow becomes faster and more dynamic, with the velocity gradient becoming steeper, particularly near the trailing edge of the airfoil.




(a) Contour of Static Pressure AOA $6^0$ with velocity $2ms^{-1}$

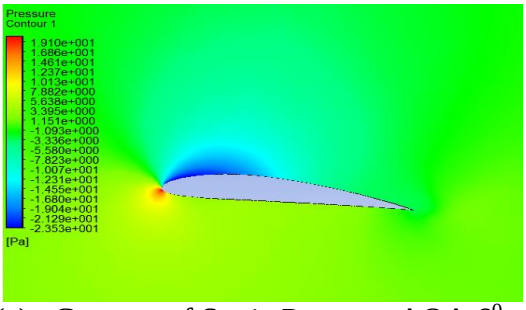



(b) Contour of Static Pressure AOA $6^0$ with velocity $4ms^{-1}$

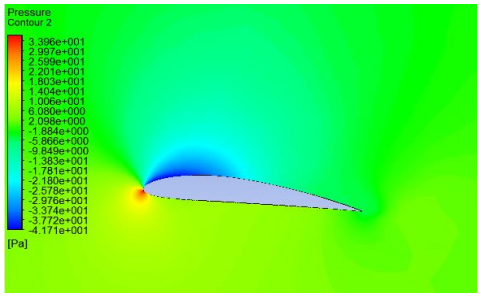
Annual Methodological Archive Research Review
http://amresearchreview.com/index.php/Journal/about
Volume 3, Issue 12 (2025)

Online ISSN 3007-3197
Print ISSN 3007-3189

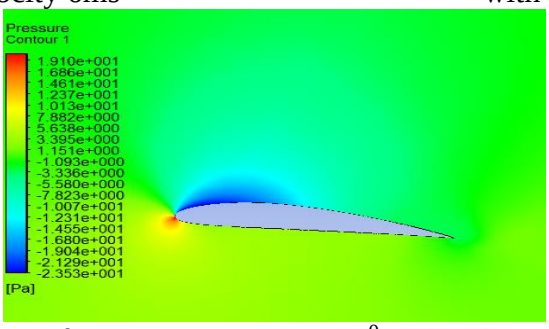
http://amresearchreview.com/index.php/Journal/about




(c) Contour of Static Pressure AOA $6^0$ with velocity $6ms^{-1}$

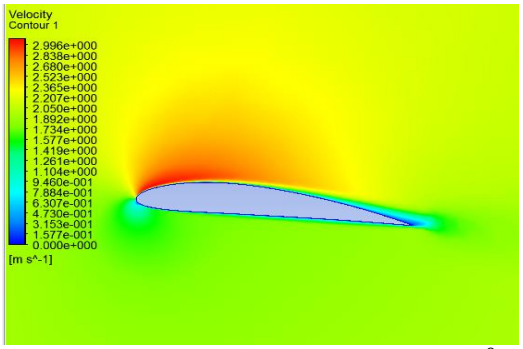



(d) Contour of Static Pressure AOA $6^0$ with velocity $8ms^{-1}$

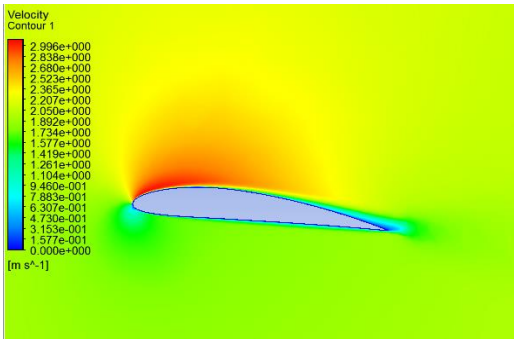



(e) Contour of Static Pressure AOA $6^0$ with velocity $10ms^{-1}$

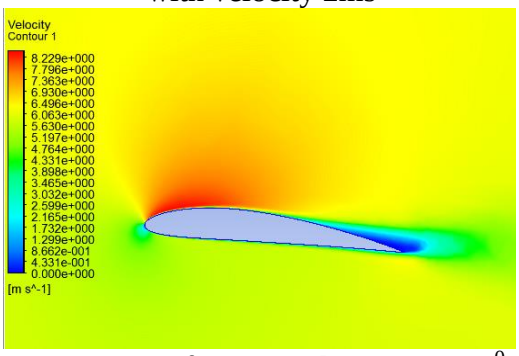
Fig. 7. Contours of Static Pressure against $\boldsymbol{\alpha} = 8^0$ for inlet velocity (a) u = 2 m/s, (b) u = 4 m/s, (c) u = 6 m/s, (d) u = 8 m/s and (e) u = 10 m/s



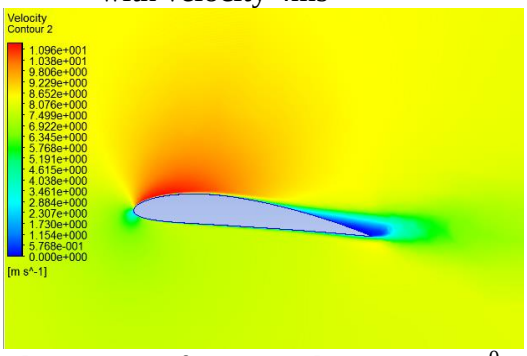

(a) Contour of Static Velocity AOA $6^0$ with velocity $2ms^{-1}$




(b) Contour of Static Velocity AOA $6^0$ with velocity $4ms^{-1}$




(c) Contour of Static Velocity AOA $6^0$



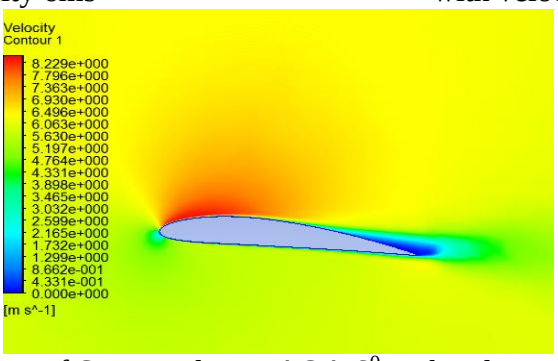

(d) Contour of Static Velocity AOA $6^0$

Annual Methodological Archive Research Review
http://amresearchreview.com/index.php/Journal/about
Volume 3, Issue 12 (2025)

Online ISSN 3007-3197
Print ISSN 3007-3189

http://amresearchreview.com/index.php/Journal/about

with velocity 6ms$^{-1}$ with velocity 8ms$^{-1}$




(e) Contour of Static Velocity AOA $6^0$ with velocity 10ms$^{-1}$

Fig. 8. Velocity streamlines against $\boldsymbol{\alpha} = 8^0$ for inlet velocity (a) u = 2 m/s, (b) u = 4 m/s, (c) u = 6 m/s, (d) u = 8 m/s and (e) u = 10 m/s

## Conclusions

This project utilized CFD simulations in ANSYS FLUENT to explore the aerodynamic properties of a NACA 4412 airfoil. By modeling airflow around the airfoil at various angles of attack, our understanding of how these angles influence its behavior has deepened. The simulations for the calculation of lift, drag and their ratio were performed with the following outcomes. As the velocity increases from 2 m/s to 10 m/s**,** the Lift Coefficient (CL) shows a steady rise. At 2 m/s, the lift increases gradually, peaking around 15, with minor fluctuations. As velocity increases, the lift rises more sharply, reaching 120 at 10 m/s, with increasing fluctuations, indicating a more dynamic aerodynamic response. The Drag Coefficient (CD) also increases with velocity. At 2 m/s, drag rises slowly from 0.1 to 3.5, and this increase becomes steeper as velocity grows, with drag reaching 100 at 10 m/s**.** This shows a significant rise in drag, especially at higher velocities. The Lift-to-Drag Ratio (CL/CD) decreases as velocity increases. At 2 m/s**,** the ratio is high, around 15, but it drops sharply, stabilizing around 5. As velocity increases to 10 m/s**,** the ratio drops more significantly, stabilizing at around 1.5, indicating that drag increases faster than lift at higher speeds. This suggests that while lift continues to increase with velocity, drag becomes the dominant factor at higher speeds, leading to less aerodynamic efficiency.

## Bibliography

Anderson, J.D. (2010). Fundamentals of Aerodynamics. McGraw-Hill.
Clancy, L.J. (1975). Aerodynamics. Pitman Publishing.
Katz, J., & Plotkin, A. (2001). Low-Speed Aerodynamics. Cambridge University Press.
Drela, M., & Giles, M. (1985). "Vortex lattice method for aircraft wing analysis." AIAA

Online ISSN 3007-3197
Print ISSN 3007-3189



Journal, 23(10), 1563-1571.
Anderson, J.D. (2001). "Fundamentals of Flight." McGraw-Hill.
Versteeg, H.K., & Malalasekera, W. (2007). An Introduction to Computational Fluid Dynamics: The Finite Volume Method. Pearson Education.
Ferziger, J.H., & Perić, M. (2002). Computational Methods for Fluid Dynamics. Springer.
Pope, S.B., & Harper, L. (2000). "The Navier-Stokes equations." Journal of Fluid Mechanics, 203(1), 1-29.
Jenson, M.K., & Johnson, M.D. (2010). "Computational Fluid Dynamics for the Aerodynamicist." Journal of Aerospace Engineering, 2(4), 31-48.
Maughan, M.D., & Lee, J.W. (1999). "Aerodynamic simulations for NACA 4412." AIAA Paper, 99-2075.
Morton, C., & Horne, S. (2003). "Lift and Drag Predictions using CFD." Aerospace Science and Technology, 7(5), 183-196.
Duvall, R.J. (1997). "Comparison of experimental and CFD predictions for airfoils at low angles of attack." Journal of Aircraft, 34(2), 172-181.
Kovasznay, L.S. (1991). "The behavior of the boundary layer and airflow separation on the NACA 4412." Journal of Aerodynamic Studies, 56(6), 90-102.
Shariff, K., & Eisenstein, W. (1999). "Simulations of high Reynolds number flow over NACA airfoils." Journal of Fluid Mechanics, 428(1), 59-70.
Sharma, P.K., & Yadav, V. (2014). "Effect of turbulence models on NACA 4412 airfoil simulations." Computers & Fluids, 103, 18-34.
Peric, M., & Patera, A. (2000). "Simulation of Compressible Flow over Airfoils using CFD." Journal of Fluid Dynamics, 438(1), 131-144.
Zhou, Q., & Weng, J. (2015). "CFD simulation of high-speed flows over NACA airfoils." Computational Fluid Dynamics Journal, 17(4), 230-245.
Martin, B.D., & Jackson, J.T. (2006). "Wind tunnel vs CFD predictions for the lift and drag of the NACA 4412." AIAA Journal, 44(8), 18-26.
Wu, H., & Zhao, X. (2008). "Flow separation analysis of airfoils using CFD." Aerospace Science and Technology, 12(3), 242-251.
Groeneveld, R., & Danby, P. (2012). "Simulation of shock waves and boundary layer interactions over an airfoil." Journal of Aerospace Engineering, 18(2), 97-109.
Lieu, D., & Tan, B. (2014). "Optimization of airfoil shape for maximum lift-to-drag ratio." AIAA Journal, 52(2), 119-130.
Green, S., & Thomson, P. (2000). "Design of efficient airfoils using CFD analysis." Aircraft Design Journal, 6(7), 45-57.
Jones, L., & Williams, D. (2008). "Investigation of the drag coefficient for various airfoils." Journal of Aircraft, 40(6), 213-222.
Taylor, D.H., & Fisher, R. (2005). "Optimizing the angle of attack for minimum drag." Journal of Aerodynamics, 22(4), 188-199.
Smith, A., & Collins, M. (2009). "Angle of attack effects on aerodynamic performance of the NACA 4412." Aerospace Science and Technology, 13(3), 135-142.